Nanoscale

Accepted Manuscript

This article can be cited before page numbers have been issued, to do this please use: S. Colford and A. Dhirani, *Nanoscale*, 2026, DOI: 10.1039/D5NR04073F.

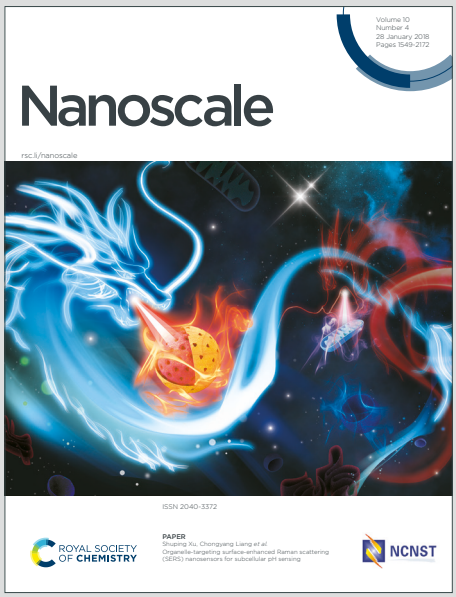

ROYAL SOCIETY OF CHEMISTRY

rsc.li/nanoscale

View Article Online
DOI: 10.1039/D5NR04073F

Using Molecular Amphiphiles to Dope Nano-Au with Cu^{2+}: 20-fold Higher Magnetic Dopant Density and Evidence for a Proximity Kondo Effect

Sean Colford ⁋ and Al-Amin Dhirani *,⁋,□

⁋ Department of Physics, University of Toronto, Toronto, Ontario, Canada, M5S 3H6.

□ Department of Chemistry, University of Toronto, Toronto, Ontario, Canada, M5S 3H6.

Email: a.dhirani@utoronto.ca

Abstract

Kondo scattering was originally observed in Au alloys containing dilute magnetic dopants. While higher densities reveal additional exotic quantum phenomena in other materials, advances combining Au and molecular systems have only increased magnetic dopant density to 0.1%. We demonstrate for the first time a doping method employing ions (Cu^{2+} or Zn^{2+}), bifunctional, amphiphilic molecular wires (4-mercaptobenzoic acid) and nano-Au systems (nano-aggregates or thin films). 1) The high surface-to-volume ratios of nanostructures and 2) the abilities for bifunctional molecules to form closely-packed, self-assembled monolayers and bind ions yield >20-fold higher densities than previously reported. We observe hallmark signatures of the Kondo effect at low temperature: the nano-aggregates magnetic moment decreases ~50-70% and film resistance increases logarithmically. Significantly, here the dopants are outside the Au, providing evidence for a “proximity” Kondo effect for the first time. These results demonstrate that quantum nanostructured materials enable a promising, bottom-up approach for exploring strongly correlated quantum phenomena.

Conduction electrons can interact with localized, magnetic moments (e.g. unpaired *d*- or *f*- electrons) to manifest a wide range of exotic quantum phenomena. The earliest example is the Kondo effect observed in the limit of low dopant density e.g. in Au films doped with magnetic, Fe impurities. Delocalized conduction electrons increasingly scatter from localized unpaired spins as the temperature decreases below a characteristic Kondo temperature (T_K), causing 1) the electrical resistance of the host material to exhibit a resistance minimum, increase logarithmically at lower temperatures and eventually saturate and 2) the magnetic moment to become screened as it forms a singlet with the conduction electrons [1,2]. Such interactions have gained renewed, intense interest as in the limit of higher densities, a number of remarkable phenomena have been observed, including high Tc superconductivity and heavy fermions[3–7].

View Article Online
DOI: 10.1039/D5NR04073F

Studying the evolution of the Kondo effect as magnetic dopant density in Au metal films increases is challenging. Simply increasing dopant levels leads to dopant clustering already at 0.01%, preventing the study of higher impurity levels in these systems[8–10]. An alternate approach that has been explored is to dope Au materials with molecules containing localized, unpaired spins[11–17]. For example, recent reports have varied the density of unpaired molecular spins using Au film – molecule – Au film layered systems, where the molecule included magnetic Co[11] or Cu [16] dopants. A maximum impurity density of ~800 ppm or 0.08% is achieved. A study using break junctions explored the coupling between delocalized electrons in Au electrodes and polypyridine ligands containing magnetic cobalt ions. Interestingly, varying the length of alkanedithiol spacers between Co and Au, the study found that Kondo effect is observed using only short linkers i.e. in the limit of strong coupling between Co ion and electrons in the Au [13]. Subsequent studies using mechanically controlled break junctions revealed that the Co ion was in 1+ spin state[14].

Nanostructures offer unique opportunities to investigate the Kondo effect in a tunable fashion. Nanoparticle properties can be controlled through size, shape and chemical composition, and molecular functionality can be controlled via chemical structure. Further, a great variety of nanostructures and their corresponding properties have been described in the literature. Among these, Au nanoparticles (NPs) functionalized with various ligands have been widely studied for their tunable optical and electronic characteristics [18–20]. Previous studies have shown that assemblies of Au NPs capped with alkanethiol molecules are magnetic, likely due to holes in Au *d*-orbitals at or near the NP surface[21–25]. The holes are generated in an uncontrolled fashion during NP synthesis and/or processing; as a result, multiple studies have reported widely varying magnetic moment values[24]. Nonetheless, studies have reported that the unpaired *d*-electrons can couple to delocalized electrons, driving a wide range of related spin-spin interactions at low temperatures[20,26].

Here, we show that we can exploit nanostructures to engineer materials to exhibit the Kondo effect at higher dopant densities than previously reported. Our approach, shown in Fig. 1, employes 4-mercaptobenzoic acid (MBA) and Au nanostructures, which are purpose-selected based on their structure-function relationships. The thiol moiety enables MBA to form densely packed self-assembled monolayers (SAMs) on Au surfaces. The benzoic acid moiety can deprotonate, and the resulting carboxylate ion can bind positive metal ions, which can be chosen to have unpaired or paired *d*-electrons, i.e. Cu^{2+} (magnetic) or Zn^{2+} (nonmagnetic, control), respectively. Finally, the short, phenyl backbone enables strong coupling between the *d*-electron and Au conduction electrons. For the Au, we employ 2 systems: films with nanoscale thickness or nanoparticles, both of which have high surface-to-volume Au atom ratios. For the films, the ratio scales as $A/At = 1/t$, where A is area and t is thickness, and for spheres

View Article Online
DOI: 10.1039/D5NR04073F

as $(4\pi r^2)/(4/3\pi r^3) \sim 1/r$, where r is sphere radius. The ratios are tunable via length scale and are high at nanoscale dimensions. As a result, ion doping with the aid of MBA self-assembly on the Au surface is expected to yield higher densities for thinner films and smaller nanoparticles.

We show here that this strategy of using surface chemistry and high surface / volume ratio of nanostructures achieves >20-fold higher localized, unpaired / delocalized electron ratios than previously reported. In addition, the strategy reveals a remarkable result for the first time. Previous observations of the Kondo effect employed dopants embedded inside tunnel junctions or films; that is, delocalized electrons traverse and scatter in the same spatial regions that localized, magnetic moments spins occupy. In contrast, the present approach employes MBA which positions the magnetic impurities outside the Au films and nanoparticles. Even in the nanoparticle aggregate case, the vast majority of magnetic impurities are near the nanoparticle surface but not in gaps between nanoparticles, as discussed further below. Nonetheless, we still observe hallmark signatures of the Kondo effect - resistance increases in films and screening of magnetic moments in the nanoparticle aggregates – providing evidence for a "proximity Kondo effect" in these materials. As such, this work not only underscores the potential for such tunable quantum nanostructured materials to serve as a platform for studying strongly correlated electron phenomena but also demonstrates a potential to reveal previously unobserved phenomena.

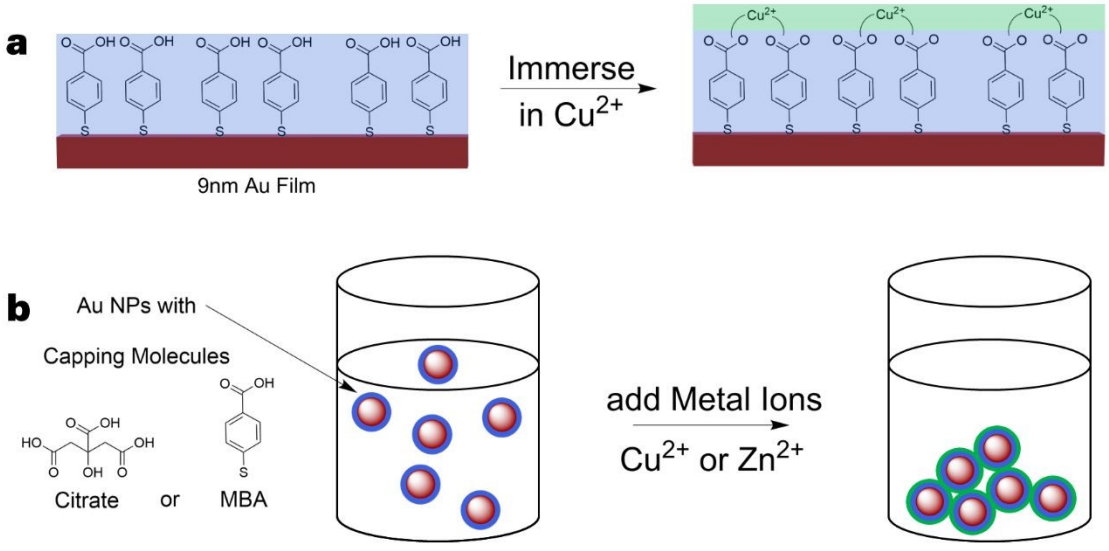

Figure 1: Schematics illustrating a) Cu^{2+} doping via a MBA self-assembled monolayer on a thermally deposited, thin Au film. b) Cu^{2+} or Zn^{2+} doping C- or MBA-capped Au NPs and forming nanostructured aggregates.

Figs. 2a and 2b show UV-Vis spectra of Au NPs both before and after addition of Cu^{2+} ions (see Supplementary Information Fig. S1 for corresponding data using Zn^{2+} ions). Before addition of the ions, citrate-capped Au NPs (C-NPs) exhibit a surface plasmon

View Article Online
DOI: 10.1039/D5NR04073F

resonance (SPR) peak centered at 530 nm. MBA-NPs exhibit an SPR peak that shifts to slightly longer wavelengths due to a change in the dielectric constant of NP surface, and an additional π - π^* transition peak near 270 nm due to the phenyl ring. Adding Cu^{2+} ions causes C- and MBA-NP SPR peaks to redshift and broaden significantly due to the increase in effective size of the nanostructured systems as ions bind to surface carboxy groups in both cases. The doubly charged ions can bind to one and, in some instances, to two C- or MBA-capping groups on different NPs, which in turn can lead to formation of NP aggregates. Figs. 2c – f show TEM images of the corresponding NPs and aggregates. The formation of large-scale aggregates upon addition of Cu^{2+} is clearly apparent. Interestingly, C-NP exhibit significant changes in individual NP sizes and shapes in the nanostructured aggregates compared with MBA-NP. This is supported by the larger and more dramatic redshift in SPR resonance of C-NPs when compared with MBA-NPs upon addition of Cu^{2+}. These data are consistent with MBA binding to Au NPs more strongly than citrate due to MBA's thiol moiety and as a result, MBA serving as a more effective NP capping molecule.

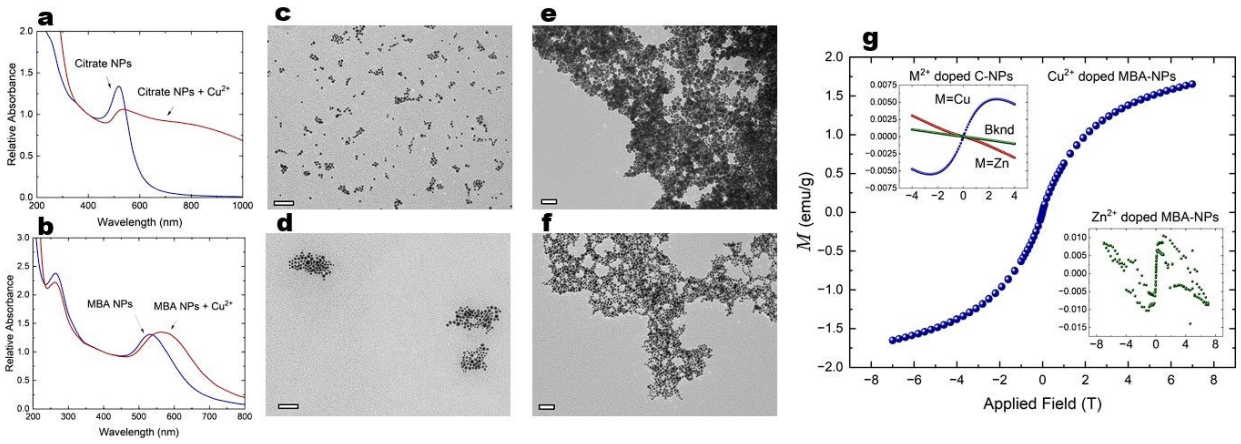

Figure 2: UV-Vis and TEM characterization of C- (top row) and MBA-NP (bottom row) solutions, NPs and aggregates. UV-Vis spectra of a) C-and b) MBA-NP solutions before and after adding Cu^{2+}. TEM images of the respective NPs c) and d) before vs. e) and f) after doping with Cu^{2+}. g) Main panel. M vs. H for Cu^{2+}-doped MBA-NP aggregates. Lower inset. M vs. H for Zn^{2+} doped MBA-NP aggregates. Upper inset. M vs. H data for Cu^{2+} and Zn^{2+} doped C-NP aggregates as well as quartz paddle + GE varnish.

Fig. 2g shows low temperature (2K) magnetic moment (M) vs. applied field (H) for C-NP and MBA-NP aggregates obtained using Zn^{2+} or Cu^{2+} ions. Aggregates obtained with Zn^{2+} exhibit weak moments, the C-NP aggregate exhibiting a diamagnetic response (Fig. 2g, both insets). The C-NP aggregate obtained with Cu^{2+} exhibits a paramagnetic response. These results are consistent with Cu^{2+} having an unpaired 3*d* electron and Zn^{2+} only paired electrons. We note that differences in the small background magnetization (~0.005 emu/g) are due to differences in the sample holders for the respective measurements. In contrast, MBA-NP aggregates obtained with Cu^{2+} exhibit a strong paramagnetic moment, ~300-fold larger than that of corresponding C-NP

View Article Online
DOI: 10.1039/D5NR04073F

aggregates. Since the citrate can desorb from the Au NP surface due to weak citrate – Au interaction, excess citrate molecules in solution are required to replenish the Au NP surface and prevent Au NP aggregation[27]. However, these excess citrate molecules can also bind to added Cu^{2+} and interfere with Cu^{2+} binding to citrates on the Au NPs surface, resulting in poorer Cu^{2+} doping. In contrast, the thiol moiety of MBA enables a strong Au-S bond, anchoring the MBA to the Au NP surface. This allows excess MBA molecules to be removed, resulting in much improved Cu^{2+} doping. We estimate that the observed magnetic moment of 1.5 emu/g for MBA-NP aggregates corresponds to 130 μ_B / Au NP. Reported values of the magnetic moment of a single copper (II) benzoate complex range between 1.4 and 1.9 μ_B depending on bond orientation[28]. This yields an estimate of ~ 70 – 90 Cu^{2+} ions per Au NP. Considering our ~4.5nm Au NPs each contain ~3,500 Au atoms (and therefore ~3,500 conduction electrons), we can conclude the impurity density in these NP aggregates is ~2-3%. XPS analysis of the Cu 2p region of similarly fabricated samples yielded a Cu^{2+} dopant density of 1.7% (see Supplementary Information Fig. S2). This is over an order of magnitude higher than the best literature values of ~0.08% using thin film molecular assemblies[11]. Raman spectroscopy has confirmed that Cu^{2+} binds to carboxyl groups on the MBA.[29]

An expected hallmark signature of Kondo scattering is screening of dopant magnetic moments at lower temperatures as unpaired *d*-electrons form singlets with delocalized electrons. To aid in analyzing the temperature response of aggregate paramagnetic behaviour, we employ the Curie Weiss law for paramagnets, $M = {B*C}/{(T-\Theta)} + M_0$ where B is the applied magnetic field, C is the Curie constant, Θ is the Weiss constant to account for the temperature scale for any transitions, and M_0 contains any offset diamagnetic contributions. C is a measure of the number and size of the moments. Figs. 3a and 4a show M vs T data for C-NP and MBA-NP aggregates, respectively, both employing Cu^{2+} ions. The small feature in C-NPs data near 80 K is attributed to an antiferromagnetic transition of trapped oxygen gas in the GE varnish. Overall, M increases rapidly at low temperature consistent with paramagnetic response expected given M *vs.* field behaviour observed at 2K. However, Figs. 3a and 4a show that fits to the data using the Curie Weiss law yield poor agreement over the entire temperature range – see insets which magnify 100-300 K region. The deviations can be readily seen by linearizing the data by plotting, ${1}/{(M-M_0)} = {(T-\Theta)}/{B*C}$. Figs. 3b and 4b show the same data as in Figs. 3a and 4a, respectively, as well as the fits using the corresponding best fit parameters. The fits clearly fail at higher temperatures. To better model the data, we assume that there are two types of paramagnetic moments and fit low temperature (2 – 50 K) and high temperature (150 – 300 K) regimes to the Curie-Weiss law separately. Figs. 3c and 4c show that this approach yields much more satisfactory agreement with the data. Fig. 3d and 4d show corresponding linearized

View Article Online
DOI: 10.1039/D5NR04073F

data and fits. In both cases, high temperature data are well described by Curie-Weiss behaviour with negative . Between ~50-80 K, there is a transition, and then low temperature data are described by another Cure-Weiss behaviour with ~50-70% larger slope (smaller C) and vanishing . Since the Curie constant, C, is a measure of the number of magnetic moments in the material[30], this analysis indicates a loss of spins as temperature decreases for both types of aggregates. We attribute the remaining paramagnetic moment observed at low temperature to approximately half of the Cu^{2+} dopants which are weakly coupled to delocalized electrons. This remaining paramagnetic moment is strong and increases as temperature decreases (Curie behaviour), dominating magnetic moment that is screened by Kondo scattering. As a result, quantitative analysis of the temperature-dependent Kondo screening and determination of the Kondo temperature is challenging with this magnetic data.

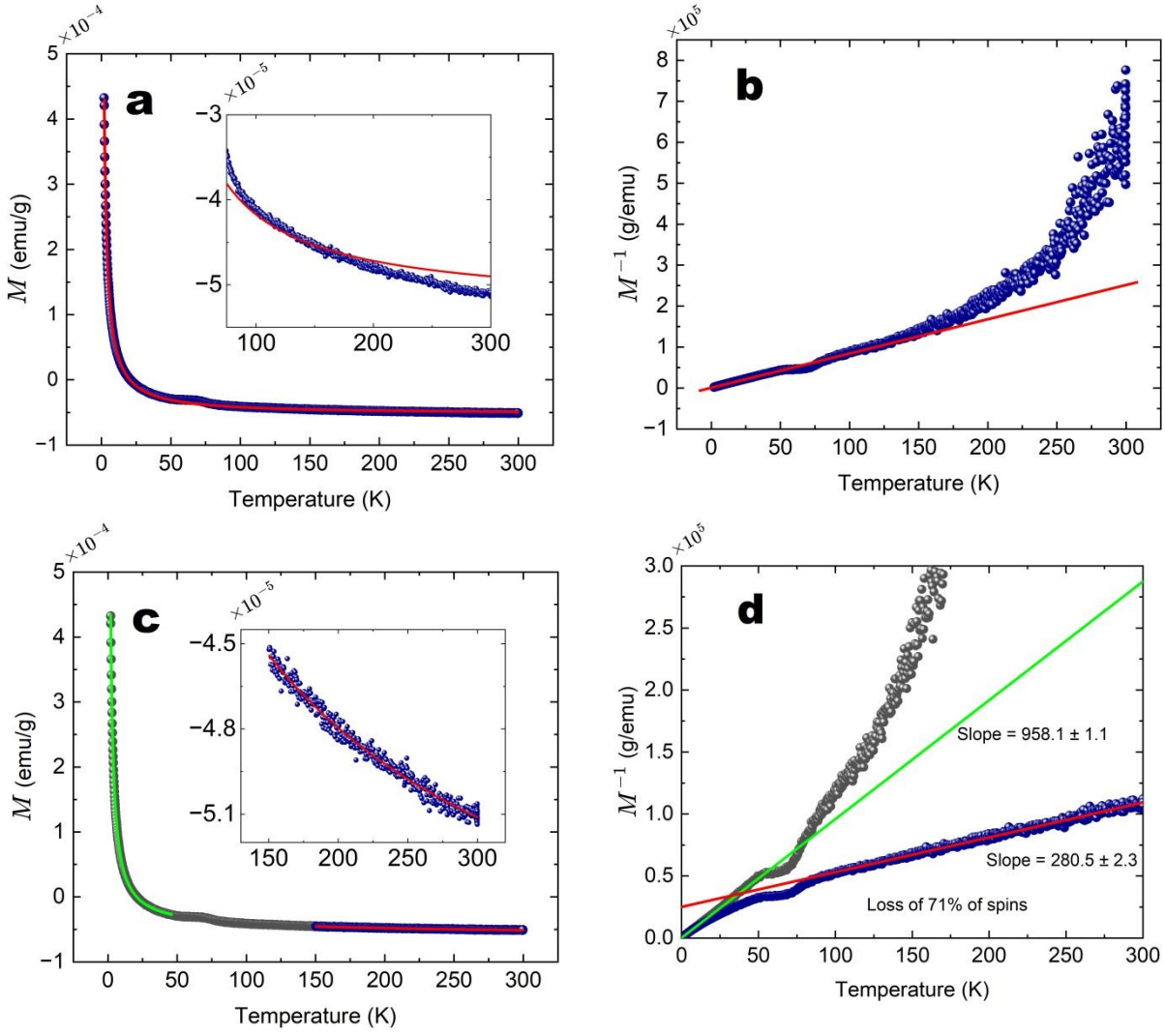

Figure 3: M vs T data and Curie-Weiss fits for a C-NP aggregate doped using Cu^{2+}. a) Single Curie-Weiss fit shown across the entire- and high-T ranges (main panel and inset, respectively). b) Linearized versions of data and fit shown

View Article Online
DOI: 10.1039/D5NR04073F

in a). c) The same data in a) with two Curie-Weiss fits at high and low temperatures shown across the entire- and high-T ranges (main panel and inset, respectively). d) Both linearized versions of this data and fits shown in c).

In the MBA-NP case, the measured value for C is much larger than that of C-NPs due to the higher density of spins; while there is less of a proportional difference between high and low T Curie constants (~50% vs ~70%), there is a much larger decrease in the total number of spins as the MBA-NP aggregate is cooled. The negative observed at higher temperatures is consistent with decreasing net magnetic moment at lower temperatures and with spin screening in Kondo materials.[31]

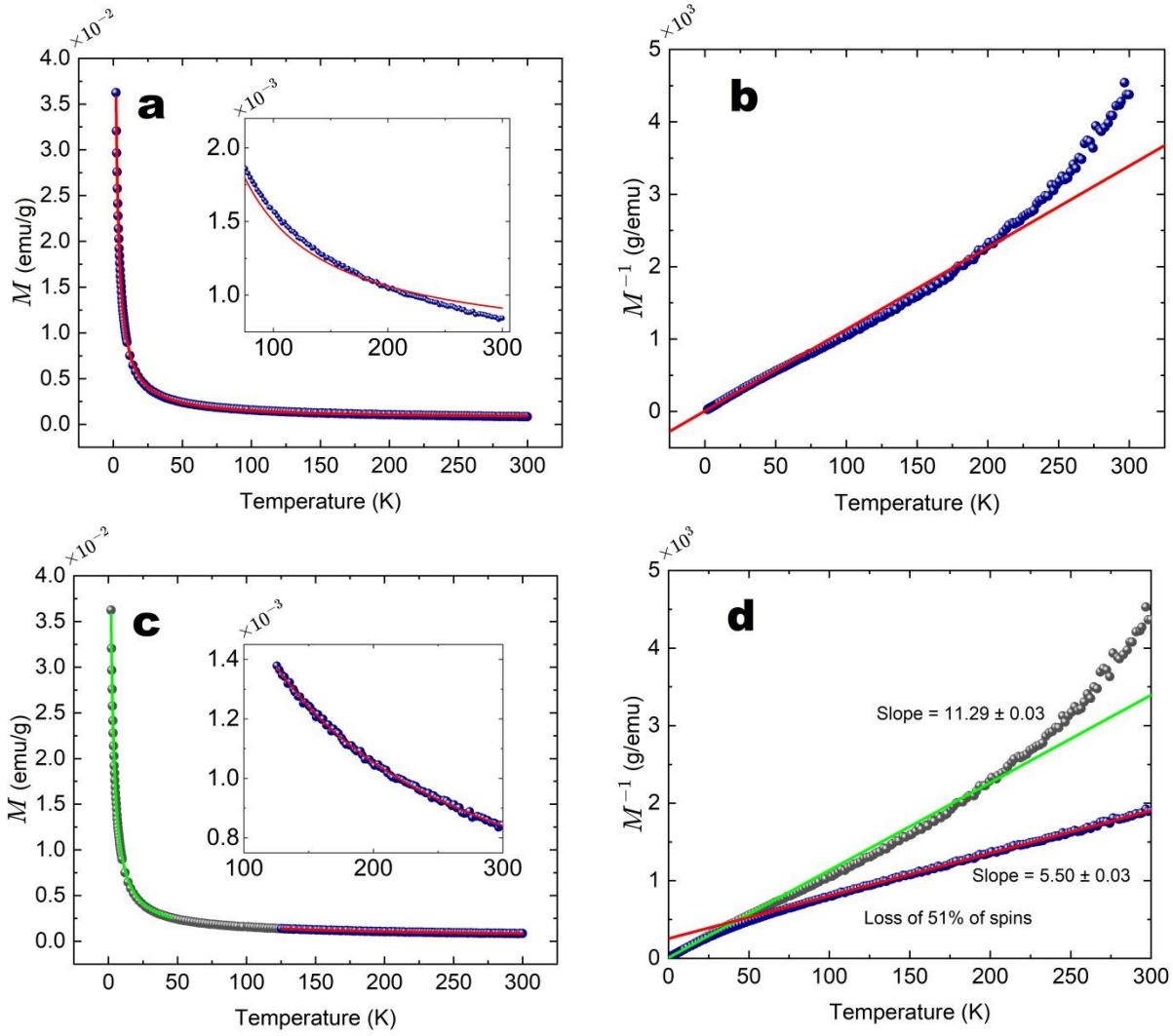

Figure 4: M vs T data and Curie-Weiss fits for a MBA-NP aggregate doped using Cu^{2+}. a) Single Curie-Weiss fit shown across the entire- and high-T ranges (main panel and inset, respectively). b) Linearized versions of data and fit shown in a). c) The same data in a) with two Curie-Weiss fits at high and low temperatures shown across the entire- and high-T ranges (main panel and inset, respectively). d) Both linearized versions of this data and fits shown in c).

View Article Online
DOI: 10.1039/D5NR04073F

Since MBA-Au aggregates have a ~300-fold higher moment density than C-Au aggregates yet both exhibit reductions in moment densities at similar temperature scales, it is not likely that interactions between unpaired *d*- electrons in Cu^{2+} dopants drive the reduction. Rather, we favor a Kondo-type screening mechanism based on interactions between delocalized Au and Cu^{2+} *d*- electrons. This is a remarkable result as the molecules incorporate the magnetic Cu^{2+} dopants outside the Au NPs. Further, for the MBA-aggregates, the number of moments/Au NP (~70-90) is at least 10-fold higher than the number of nearest neighbor Au NPs, given that the aggregates are disordered and porous; that is, many Cu^{2+} dopants are bound to MBA on single NP surfaces rather than sandwiched between two MBA molecules between NPs. These results provide evidence for a "proximity" Kondo mechanism in which Au electrons scatter off *d*- electrons in Cu^{2+} ions, with the Cu^{2+} located outside the Au NP and near the surface.

To test this hypothesis, we measured R *vs*. T of 8 nm-thick Au films before and after depositing MBA SAMs and doping with Cu^{2+} ions near the films' surfaces and test for an expected second hallmark signature of Kondo scattering, namely a logarithmic resistance upturn at low temperature. We characterized the binding of Cu^{2+} to MBA molecules by conducting Cyclic Voltammetry using 50 nm Au films – see Fig. 5a. The initial negative voltage sweep direction generates a large negative cathodic peak related to Cu^{2+} to Cu^{1+} reduction, and the subsequent positive voltage sweeps generates a broader and smaller positive anodic peak related to Cu^{1+} to Cu^{2+} oxidation, in agreement with previous reports[32]. As a control, Fig. 5a shows that bare Au films (no MBA) that are exposed to Cu^{2+} ions do not exhibit Cu^{2+}/Cu^{1+} redox features. The Cu^{2+}/Cu^{1+} redox couple confirms the presence of electrochemically active Cu ions immobilized by the SAM near the Au surface and their initial state before electrochemistry is Cu^{2+}. This is also confirmed by previous XPS studies of NP films coated with MBA which capture Cu^{2+} ions .

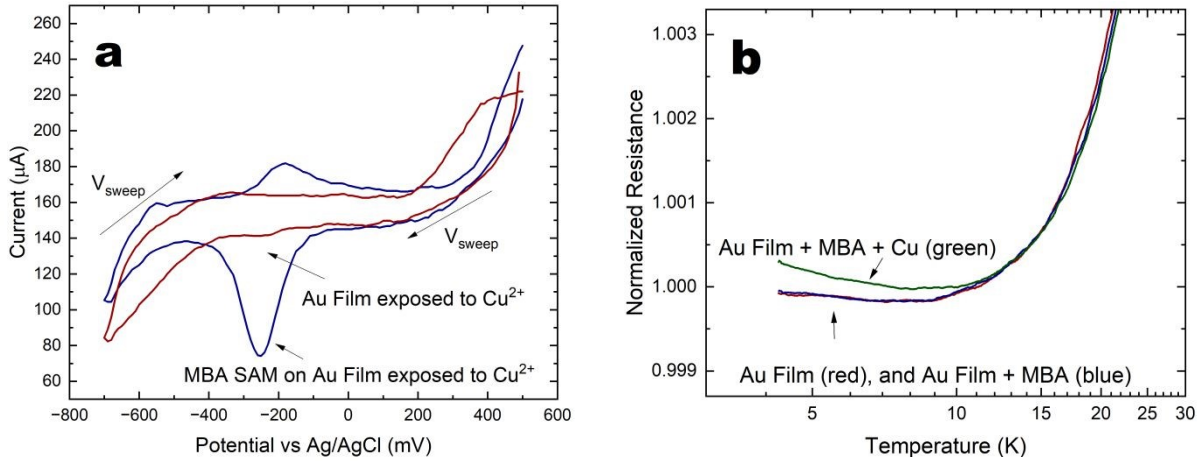

View Article Online
DOI: 10.1039/D5NR04073F

Figure 5: a) Current vs. potential electrochemical cyclic voltammograms obtained using two Au films - with and without an MBA SAM – both after doping with Cu^{2+}. Data are obtained at room temperature using a triangular potential scan at 0.05 $\frac{V}{s}$ and purged aqueous 0.1 M phosphate buffer (pH 7.4). b) R vs T of the same Au film at different stages of Cu^{2+} doping: bare film (red), after depositing an MBA SAM (blue), and subsequently doping with Cu^{2+} (green). A resistance increase only after Cu^{2+} immersion is apparent below 10 K. Here we normalized all data to 12 K.

We measured the 4-probe *R* vs *T* of these films down to 4 K – Fig. 5b. Film resistances for bare and SAM-coated Au films decrease down to ~15 K due to reduced phonon scattering then plateau due to residual defect scattering. As anticipated, the SAM-coated Au film doped with Cu^{2+} exhibits a pronounced resistance increase proportional to log *T* below
~10 K. We note that some bare Au films exhibited a low temperature upturn and exposure to Cu^{2+} (no SAM) led to a slight increase due to small physisorption; however, for 5 of 6 samples, adding an MBA SAM and doping with Cu^{2+} led to significant, further low temperature increases as shown. See Supplementary Information Fig. S2 for additional Au film + MBA monolayer sample, and corresponding data without assembling MBA monolayer as control. Combined, magnetic moment screening and log *T* resistance increase at low temperature suggests a proximity Kondo effect in these nanostructured systems[30,33].

In disordered thin films, a resistance upturn at low temperatures can be driven by electron localization phenomena.[34] To probe such phenomena, we measured magnetoresistance at 4 K first using bare Au films, then again using the same films with MBA SAM's, and finally using the same films after immersing in Cu^{2+} or Zn^{2+} solutions (see Supplementary Information Fig. S4). Resistance increases with magnetic field in all samples. These results are consistent with localization contributing to magnetoresistance and *R* vs *T* upturn observed in samples. However, we observe that magnetoconductance does not change significantly after doping with Cu^{2+} or Zn^{2+}, indicating localization is not significantly modified in the film. This is supported by Raman analysis which shows that Cu^{2+} binds to the carboxy group on the MBA, as mentioned above. Since doping with Cu^{2+} causes the *R* vs *T* upturn to increase in a majority of samples tested, our results suggest that localization cannot entirely account for the *R* vs *T* upturn increase.

The present experiment is closely related to electrochemically-driven charge transfer, in a common situation where redox molecules closely approach electrodes. A recent study[35] reports that as metallocene complexes approach a thin film Au electrode, Au band and molecule states overlap and can hybridize. At the redox potential, local electric field in the surface charge double later shifts molecule redox-active states to the

View Article Online
DOI: 10.1039/D5NR04073F

Au Fermi level where charge transfer can occur and hybridization leads to a resistance increase (delocalized electrons adopt a localized character). After excluding Joule heating, this mechanism is used to explain an observed correlation between redox current and spikes in resistance, which is otherwise difficult to rationalize for an Ohmic metal film. In the present experiment, Kondo scattering and low temperature resistance increase may also be viewed as being caused by hybridization between delocalized electrons at the Fermi level and localized, unpaired electrons, albeit at lower energies via a second order interaction. In both experiments, such strong interactions are possible even when the localized state is outside but near the metal. As such, the proximity Kondo effect described here and electrochemical redox, which is of significant scientific and technological interest, provide reinforcing pictures when viewed through a quantum perspective.

Acknowledgements

The authors acknowledge funding from the natural Sciences and Engineering Research Council of Canada and MITACS.

References

(1) Kondo, J.; Laboratory, E. Resistance Minimum in Dilute Magnetic Alloys. *Prog. Theor. Phys.* **1964**, *32*, 37. https://doi.org/10.1143/PTP.32.37.
(2) Sarachik, M. P.; Corenzwit, E.; Longinotti, L. D. Resistivity of Mo-Nb and Mo-Re Alloys Containing 1% Fe. *Phys. Rev.* **1964**, *135* (4A), A1041–A1045. https://doi.org/10.1103/PhysRev.135.A1041.
(3) Lee, P. A.; Nagaosa, N.; Wen, X.-G. Doping a Mott Insulator: Physics of High-Temperature Superconductivity. *Rev. Mod. Phys.* **2006**, *78* (1), 17–85. https://doi.org/10.1103/RevModPhys.78.17.
(4) Wirth, S.; Steglich, F. Exploring Heavy Fermions from Macroscopic to Microscopic Length Scales. *Nat Rev Mater* **2016**, *1* (10), 16051. https://doi.org/10.1038/natrevmats.2016.51.
(5) Imada, M.; Fujimori, A.; Tokura, Y. Metal-Insulator Transitions. *Rev. Mod. Phys.* **1998**, *70* (4), 1039–1263. https://doi.org/10.1103/RevModPhys.70.1039.
(6) Georges, A.; Kotliar, G.; Krauth, W.; Rozenberg, M. J. Dynamical Mean-Field Theory of Strongly Correlated Fermion Systems and the Limit of Infinite Dimensions. *Rev. Mod. Phys.* **1996**, *68* (1), 13–125. https://doi.org/10.1103/RevModPhys.68.13.
(7) Basov, D. N.; Averitt, R. D.; Van Der Marel, D.; Dressel, M.; Haule, K. Electrodynamics of Correlated Electron Materials. *Rev. Mod. Phys.* **2011**, *83* (2), 471–541. https://doi.org/10.1103/RevModPhys.83.471.
(8) Ford, P. J.; Whall, T. E.; Loram, J. W. Effect of Interactions on the Kondo Resistivity of Dilute Au Fe Alloys. *Phys. Rev. B* **1970**, *2* (6), 1547–1553. https://doi.org/10.1103/PhysRevB.2.1547.
(9) Chen, G.; Giordano, N. Thickness Dependence of the Kondo Effect in AuFe Films. *Phys. Rev. Lett.* **1991**, *66* (2), 209–211. https://doi.org/10.1103/PhysRevLett.66.209.

View Article Online
DOI: 10.1039/D5NR04073F

(10) Eisenmenger, J.; Meckler, J.; Ziemann, P. Kondo Effect and Local Disorder in Ion Irradiated AuFe. *Journal of Low Temperature Physics* **2004**, *137* (3–4), 167–178. https://doi.org/10.1023/B:JOLT.0000049051.91441.06.
(11) Gang, T.; Yilmaz, M. D.; Ataç, D.; Bose, S. K.; Strambini, E.; Velders, A. H.; Jong, M. P. de; Huskens, J.; Wiel, W. G. van der. Tunable Doping of a Metal with Molecular Spins. *Nature Nanotech* **2012**, *7* (4), 232–236. https://doi.org/10.1038/nnano.2012.1.
(12) Liang, W.; Shores, M. P.; Bockrath, M.; Long, J. R.; Park, H. Kondo Resonance in a Single-Molecule Transistor. *Nature* **2002**, *417* (6890), 725-.
(13) Park, J.; Pasupathy, A. N.; Goldsmith, J. I.; Chang, C.; Yaish, Y.; Petta, J. R.; Rinkoski, M.; Sethna, J. P.; Abruña, H. D.; McEuen, P. L.; Ralph, D. C. Coulomb Blockade and the Kondo Effect in Single-Atom Transistors. *Nature* **2002**, *417* (6890), 722–725. https://doi.org/10.1038/nature00791.
(14) Parks, J. J.; Champagne, A. R.; Costi, T. A.; Shum, W. W.; Pasupathy, A. N.; Neuscamman, E.; Flores-Torres, S.; Cornaglia, P. S.; Aligia, A. A.; Balseiro, C. A.; Chan, G. K.-L.; Abruña, H. D.; Ralph, D. C. Mechanical Control of Spin States in Spin-1 Molecules and the Underscreened Kondo Effect. *Science* **2010**, *328* (5984), 1370–1373.
(15) Zhang, Y.; Kahle, S.; Herden, T.; Stroh, C.; Mayor, M.; Schlickum, U.; Ternes, M.; Wahl, P.; Kern, K. Temperature and Magnetic Field Dependence of a Kondo System in the Weak Coupling Regime. *Nat Commun* **2013**, *4* (1), 2110. https://doi.org/10.1038/ncomms3110.
(16) Atxabal, A.; Ribeiro, M.; Parui, S.; Urreta, L.; Sagasta, E.; Sun, X.; Llopis, R.; Casanova, F.; Hueso, L. E. Spin Doping Using Transition Metal Phthalocyanine Molecules. *Nat Commun* **2016**, *7* (1), 13751. https://doi.org/10.1038/ncomms13751.
(17) Yu, L. H.; Natelson, D. The Kondo Effect in C_{60} Single-Molecule Transistors. *Nano Lett.* **2004**, *4* (1), 79–83. https://doi.org/10.1021/nl034893f.
(18) Gravelsins, S.; Park, M. J.; Niewczas, M.; Hyeong, S.-K.; Lee, S.-K.; Ahmed, A.; Dhirani, A.-A. Large Emergent Optoelectronic Enhancement in Molecularly Cross-Linked Gold Nanoparticle Nanosheets. *Commun Chem* **2022**, *5* (1), 103. https://doi.org/10.1038/s42004-022-00723-2.
(19) Zamborini, F. P.; Hicks, J. F.; Murray, R. W. Quantized Double Layer Charging of Nanoparticle Films Assembled Using Carboxylate/(Cu^{2+} or Zn^{2+})/Carboxylate Bridges. *J. Am. Chem. Soc.* **2000**, *122* (18), 4514–4515. https://doi.org/10.1021/ja0006696.
(20) Tie, M.; Colford, S.; Niewczas, M.; Baumbach, R.; Dhirani, A.-A. Widely Varying Kondo and Magnetic Interactions in Molecule Gold Nanostructured Materials by Changing the Gold Nanoarchitecture. *Nano Lett.* **2023**, *23* (9), 3724–3730. https://doi.org/10.1021/acs.nanolett.2c04918.
(21) Dutta, P.; Pal, S.; Seehra, M. S.; Anand, M.; Roberts, C. B. Magnetism in Dodecanethiol-Capped Gold Nanoparticles: Role of Size and Capping Agent. *Applied Physics Letters* **2007**, *90* (21), 213102. https://doi.org/10.1063/1.2740577.
(22) Crespo, P.; Litrán, R.; Rojas, T. C.; Multigner, M.; de la Fuente, J. M.; Sánchez-López, J. C.; García, M. A.; Hernando, A.; Penadés, S.; Fernández, A. Permanent Magnetism, Magnetic Anisotropy, and Hysteresis of Thiol-Capped Gold

View Article Online
DOI: 10.1039/D5NR04073F

Nanoparticles. *Phys. Rev. Lett.* **2004**, *93* (8), 087204. https://doi.org/10.1103/PhysRevLett.93.087204.
(23) Garitaonandia, J. S.; Insausti, M.; Goikolea, E.; Suzuki, M.; Cashion, J. D.; Kawamura, N.; Ohsawa, H.; Gil de Muro, I.; Suzuki, K.; Plazaola, F.; Rojo, T. Chemically Induced Permanent Magnetism in Au, Ag, and Cu Nanoparticles: Localization of the Magnetism by Element Selective Techniques. *Nano Lett.* **2008**, *8* (2), 661–667. https://doi.org/10.1021/nl073129g.
(24) Nealon, G. L.; Donnio, B.; Greget, R.; Kappler, J.-P.; Terazzi, E.; Gallani, J.-L. Magnetism in Gold Nanoparticles. *Nanoscale* **2012**, *4* (17), 5244–5258. https://doi.org/10.1039/C2NR30640A.
(25) Guerrero, E.; Muñoz-Márquez, M. A.; García, M. A.; Crespo, P.; Fernández-Pinel, E.; Hernando, A.; Fernández, A. Surface Plasmon Resonance and Magnetism of Thiol-Capped Gold Nanoparticles. *Nanotechnology* **2008**, *19* (17), 175701. https://doi.org/10.1088/0957-4484/19/17/175701.
(26) Tie, M.; Gravelsins, S.; Niewczas, M.; Dhirani, A.-A. Large Kondo Effect in Assemblies of Au Nanoparticles Linked with Alkanedithiol Electron Bridges. *Nanoscale* **2019**, *11* (12), 5395–5401. https://doi.org/10.1039/C8NR09280J.
(27) La Spina, R.; Spampinato, V.; Gilliland, D.; Ojea-Jimenez, I.; Ceccone, G. Influence of Different Cleaning Processes on the Surface Chemistry of Gold Nanoparticles. *Biointerphases* **2017**, *12* (3), 031003. https://doi.org/10.1116/1.4994286.
(28) Inoue, M.; Kishita, M.; Kubo, M. Magnetic Moments of Copper(II) Salicylate, Copper(II) Benzoate, and Some Related Compounds. *Inorg. Chem.* **1964**, *3* (2), 239–242. https://doi.org/10.1021/ic50012a022.
(29) Colford, S.; Dhirani, A.-A. Detection of Cu2+ Ion with 100-Fold Improvement Using Mercaptobenzoic Acid-Capped Au Nanoparticles Purified by pH Selective Precipitation. *Colloids and Surfaces A: Physicochemical and Engineering Aspects* **2025**, *723*, 137416. https://doi.org/10.1016/j.colsurfa.2025.137416.
(30) Luo, Y.; Pourovskii, L.; Rowley, S. E.; Li, Y.; Feng, C.; Georges, A.; Dai, J.; Cao, G.; Xu, Z.; Si, Q.; Ong, N. P. Heavy-Fermion Quantum Criticality and Destruction of the Kondo Effect in a Nickel Oxypnictide. *Nature Mater* **2014**, *13* (8), 777–781. https://doi.org/10.1038/nmat3991.
(31) Lv, B.; Chen, J.; Qiao, L.; Ma, J.; Yang, X.; Li, M.; Wang, M.; Tao, Q.; Xu, Z.-A. Magnetic and Transport Properties of Low-Carrier-Density Kondo Semimetal CeSbTe. *J. Phys.: Condens. Matter* **2019**, *31* (35), 355601. https://doi.org/10.1088/1361-648X/ab2498.
(32) Urcuyo, R.; Cortés, E.; Rubert, A. A.; Benitez, G.; Montero, M. L.; Tognalli, N. G.; Fainstein, A.; Vela, M. E.; Salvarezza, R. C. Aromatic and Aliphatic Thiol Self-Assembled Monolayers on Au: Anchoring and Delivering Copper Species. *J. Phys. Chem. C* **2011**, *115* (50), 24707–24717. https://doi.org/10.1021/jp207875g.
(33) Ghosh, K.; Ramakrishnan, S.; Malik, S. K.; Chandra, G. Resistivity and Magnetic-Susceptibility Studies in the *R* Pd 2 Al 3 (*R* =La, Ce, Pr, Nd, and Sm) System. *Phys. Rev. B* **1993**, *48* (9), 6249–6254. https://doi.org/10.1103/PhysRevB.48.6249.
(34) Abrahams, E. *50 Years of Anderson Localization*; WORLD SCIENTIFIC, 2010. https://doi.org/10.1142/7663.

View Article Online
DOI: 10.1039/D5NR04073F

(35) Chen, X.; Dhirani, A.-A. Thin Film Resistance Gating by Redox Charge Exchange: Evidence for a Quantum Transition State. *ACS Appl. Mater. Interfaces* **2024**, *16* (19), 25540–25550. https://doi.org/10.1021/acsami.4c02058.

View Article Online
DOI: 10.1039/D5NR04073F

Data availability

All data supporting the findings of this study are included within the article and the Supplementary Information. No additional source data are required.